Supplement of Atmos. Chem. Phys., 17, 13187–13211, 2017
https://doi.org/10.5194/acp-17-13187-2017-supplement

Atmospheric Chemistry and Physics
Open Access
EGU

Supplement of

Kinetic modeling studies of SOA formation from α-pinene ozonolysis

Kathrin Gatzsche et al.

Correspondence to: Kathrin Gatzsche (gatzsche@tropos.de)

1 Gas-phase chemistry mechanism for α-pinene oxidation

Table S1: Reaction mechanism for the degradation of α-pinene according to Chen and Griffin (2005) updated by rate constants from MCM and HOM yields.

#	Reactants		Products	Rate constant in $cm^3\ molecule^{-1}\ s^{-1}$	Ref.
1a	APIN + OH	$\rightarrow$	$RO_2$101 + RO_2T	1.21E-11$\times\exp(444/T)$	1, 6
1b	APIN + OH	$\rightarrow$	0.961 $RO_2$101 + 0.961 RO_2T + 0.024 HOM†	1.21E-11$\times\exp(444/T)$	1, 6
2	APIN + NO_3	$\rightarrow$	$RO_2$102 + RO_2T	1.2E-12$\times\exp(490/T)$	1, 6
3a	APIN + O_3	$\rightarrow$	0.2 $RO_2$103 + 0.2 CO + 0.8 OH + 0.05 UR101 + 0.15 PINA + 0.15 H_2O_2 + 0.33 $RO_2$104 + 0.27 $RO_2$105 + 0.8 RO_2T	8.05E-16$\times\exp(640/T)$	1, 6
3b	APIN + O_3	$\rightarrow$	0.1932 $RO_2$103 + 0.1932 CO + 0.7728 OH + 0.0483 UR101 + 0.1449 PINA + 0.1449 H_2O_2 + 0.31878 $RO_2$104 + 0.26082 $RO_2$105 + 0.034 HOM†	8.05E-16$\times\exp(640/T)$	1, 6
4	APIN + O3PX	$\rightarrow$	0.75 UR103 + 0.25 NOPI	3.2E-11	2
5	$RO_2$101 + NO	$\rightarrow$	0.2 AP101 + 0.6 PINA + 0.8 HO_2 + 0.2 KETH + 0.2 HCHO	8.8E-13$\times\exp(180.2/T)$	2
6	$RO_2$101 + RO_2T	$\rightarrow$	0.7 PINA + HO_2 + 0.3 UR107 + O_2	1.82E-13$\times\exp(416/T)$	2
7	$RO_2$101 + HO_2	$\rightarrow$	0.8 PINA + 0.2 KETH + 0.2 HCHO + OOH1	4.1E-13$\times\exp(790/T)$	2
8	$RO_2$102 + NO	$\rightarrow$	0.6 PINA + 1.825 NO_2 + 0.175 AP102 + 0.225 KETH + 0.225 HCHO + 0.4 HO_2	8.8E-13$\times\exp(180.2/T)$	2
9	$RO_2$102 + RO_2T	$\rightarrow$	0.795 PINA + 0.795 NO_2 + 0.135 AP101 + 0.07 AP102 + O_2	1.82E-13$\times\exp(416/T)$	2
10	$RO_2$102 + HO_2	$\rightarrow$	0.6 PINA + 0.825 NO_2 + 0.175 AP102 + 0.225 HCHO + 0.225 HO_2 + 0.175 OOH1 + 0.825 OOH2	4.1E-13$\times\exp(790/T)$	2
11	$RO_2$103 + NO	$\rightarrow$	0.38 AP103 + 0.62 NRPA + 0.62 HO_2 + 0.62 NO_2	1.05E-12$\times\exp(180.2/T)$	2, a
12	$RO_2$103 + RO_2T	$\rightarrow$	NRPA + HO_2 + O_2	1.82E-13$\times\exp(416/T)$	2
13	$RO_2$103 + HO_2	$\rightarrow$	NRPA + OOH1	4.1E-13$\times\exp(790/T)$	2
14	$RO_2$104 + NO	$\rightarrow$	NO_2 + $RO_2$108 + $RO_2$8	8.8E-13$\times\exp(180.2/T)$	2
15	$RO_2$104 + RO_2T	$\rightarrow$	0.7 $RO_2$108 + 0.7 $RO_2$8 + 0.3 RP102 + O_2	1.82E-13$\times\exp(416/T)$	2

16	$RO_2$104 + HO_2	→	$RO_2$108 + $RO_2$8 + OOH2	4.1E-13 × exp (790/T)	2
17	$RO_2$105 + NO	→	HCHO + NO_2 + $RO_2$109	8.8E-13 × exp (180.2/T)	2
18	$RO_2$105 + RO_2T	→	0.8 HCHO + 0.8 $RO_2$109 + 0.10 UR105 + 0.05 RP103 + 0.05 UR108 + O_2	1.82E-13 × exp (416/T)	2
19	$RO_2$105 + HO_2	→	HCHO + $RO_2$109 + OOH2	4.1E-13 × exp (790/T)	2
20	PINA + hν	→	CO + HO_2 + $RO_2$103	Photolysis MCM*	6, 7
21	PINA + OH	→	0.8 $RO_2$106 + 0.2 RO2104 + H_2O	9.1E-11	4
22	PINA + NO_3	→	$RO_2$106 + HNO_3	5.4E-14	4
23	$RO_2$106 + NO	→	$RO_2$103 + 0.8 CO_2 + O_2	1.11-11 × exp (180.2/T)	2
24	$RO_2$106 + NO_2 + M	→	PAN101 + M	see Griffin et al. (2002)	3
25	PAN101	→	$RO_2$106 + NO_2	see Griffin et al. (2002)	3
26	$RO_2$106 + RO_2T	→	0.2 UR101 + 0.8 $RO_2$103 + 0.8 CO_2 + O_2	5.0E-12	2
27	$RO_2$106 + HO_2	→	0.2 UR101 + O_3	4.3E-13 × exp (1040/T)	2
28	NRPA + hν	→	CO + HO_2 + $RO_2$108	Photolysis MCM*	6, 7
29	NRPA + OH	→	0.8 $RO_2$107 + 0.2 $RO_2$104 + H_2O	9.1E-11	4
30	NRPA + NO_3	→	$RO_2$107 + HNO_3	5.4E-14	4
31	$RO_2$107 + NO	→	NO_2 + CO_2 + $RO_2$108	1.11-11 × exp (180.2/T)	2
32	$RO_2$107 + NO_2 + M	→	PAN102 + M	see Griffin et al. (2002)	3
33	PAN102	→	$RO_2$107 + NO_2	see Griffin et al. (2002)	3
34	$RO_2$107 + RO_2T	→	0.2 UR102 + 0.8 CO_2 + 0.87,$RO_2$108 + O_2	5.0E-12	2
35	$RO_2$107 + HO_2	→	UR102 + O_3	4.3E-13 × exp (1040/T)	2
36	$RO_2$108 + NO	→	0.35 AP104 + 0.65 KETH + 0.65 NO_2 + 0.65 HO_2	1.24E-12 × exp (180.2/T)	2, a
37	$RO_2$108 + RO_2T	→	KETH + HO_2 + O_2	1.82E-13 × exp (416/T)	2
38	$RO_2$108 + HO_2	→	KETH + OOH1	4.1E-13 × exp (790/T)	2
39	$RO_2$109 + NO	→	CO_2 + NO_2 + $RO_2$108	1.11-11 × exp (180.2/T)	2
40	$RO_2$109 + NO_2 + M	→	PAN103 + M	see Griffin et al. (2002)	3
41	PAN103	→	$RO_2$109 + NO_2	see Griffin et al. (2002)	3
42	$RO_2$109 + RO_2T	→	0.3 RP101 0.1 UR104 + 0.6 CO_2 + 0.6 $RO_2$108 + O_2	5.0E-12	2
43	$RO_2$109 + HO_2	→	UR104 + O_2	4.3E-13 × exp (1040/T)	2
44	AP101 + OH	→	PINA + NO_2 + H_2O	5.63E-12	5
45	AP102 + OH	→	$RO_2$108 + NO_2 + H_2O	6.86E-12	5
46	AP103 + OH	→	NRPA + NO_2 + H_2O	2.53E-12	5
47	AP104 + OH	→	KETH + NO_2 + H_2O	2.02E-12	5
48	RP101 + OH	→	UR104 + O_3 - HO_2	2.62E-11	5
49	RP102 + OH	→	UR106 + O_3 - HO_2	2.36E-11	5

50	RP103 + OH	$\rightarrow$ UR105 + O_3 - HO_2	2.66E-11	5

† Reactions updated by HOM yields according to Berndt et al. (2016) utilized for cases 5a and 5b of Table 1

a) Yields calculated according to Arey et al. (2001)

References: 1) Atkinson (1997); 2) Jenkin et al. (1997); 3) Griffin et al. (2002); 4) Glasius et al. (1997); 5) Kwok and Atkinson (1995); 6) http://mcm.leeds.ac.uk/MCM/; 7) Saunders et al. (2003)

* Photolysis according to Saunders et al. (2003) with $J = l(\cos(\chi))^m \exp(-n \sec \chi)$ with χ the solar zenith angle; l = 2.792E-05; m = 0.805; n = 0.338.

Table S2: Abbreviations and full names of the chemical species included in the α-pinene oxidation mechanism.

Term	**Description**
	Reactive, fully integrated species
APIN	α-pinene
PINA	pinonaldehyde
NRPA	norpinonaldehyde
AP101	2-nitrato-3-hydroxy-pinane
AP102	2-nitrato-3-oxo-pinane
AP103	2,2-dimethyl-3-acetyl-cyclobutyl-methyl-nitrate
AP104	2,2-dimethyl-3-acetyl-cyclobutyl-nitrate
HOM	highly oxidized organic compound
PAN101	peroxy 2,2-dimethyl-3-acetyl-cyclobutyl-acetyl-nitrate
PAN102	peroxy 2,2-dimethyl-3-acetyl-cyclobutyl-formyl-nitrate
PAN103	peroxy 2,2-dimethyl-3-formylmethyl-cyclobutyl-formyl-nitrate
RP101	pinalic-3-acid
RP102	1-hydroxy-pinonaldehyde
RP103	10-hydroxy-pinonaldehyde
	Nonreacting, fully integrated species
UR101	pinonic acid
UR102	norpinonic acid
UR103	2,3-pinane-epoxide
UR104	pinic acid
UR105	10-hydroxy-pinonic acid
UR106	1-hydroxy-pinonic acid
UR107	2,3-dihydroxy-pinane

UR108	2-(2,2-dimethyl-3-formylmethyl-cyclobutyl)-2-keto-acetaldehyde
	Reactive, organic pseudo-steady species
RO_2101	hydroxy alkyl peroxy radical from oxidation of α-pinene (2-peroxy-3-hydroxy-pinane)
RO_2102	nitrato alkyl peroxy radical from oxidation of α-pinene (65 % is 2-peroxy-3-nitrato-pinane, 35 % is 2-nitrato-3-peroxy-pinane)
RO_2103	cyclic keto alkyl peroxy radical from oxidation of α-pinene (C_4 cycle, 1-methyl peroxy, 2,2-dimethyl, 3-acetyl)
RO_2104	cyclic keto aldehydic peroxy radical from oxidation of α-pinene (C_4 cycle, 1-peroxy, 1-acetyl, 2,2-dimethyl, 3-formylmethyl)
RO_2105	cyclic keto alkyl peroxy radical from oxidation of α-pinene (C_4 cycle, 1-(1-keto-ethyl peroxy), 2,2-dimethyl, 3-formylmethyl)
RO_2106	acyl peroxy radical from aldehydic H abstraction of pinonaldehyde
RO_2107	acyl peroxy radical from aldehydic H abstraction of norpinonaldehyde
RO_2108	cyclic keto alkyl peroxy radical from oxidation of α-pinene (C_4 cycle, 1-peroxy, 2,2-dimethyl, 3-acetyl)
RO_2109	acyl peroxy radical from oxidation of α-pinene (C_4 cycle, 1-formyl peroxy, 2,2-dimethyl, 3-formylmethyl)

Table S3: Considered particle phase reactions for α-pinene oxidized products required for the kinetic approach and added to the reaction mechanism presented in Table S1.

#	Reactants		Products	Rate constant in s^{-1}
51	pPINA	$\rightarrow$	rPINA	$1-10^{-6}$
52	pRP101	$\rightarrow$	rRP101	$1-10^{-6}$
53	pUR104	$\rightarrow$	rUR104	$1-10^{-6}$
54	pNRPA	$\rightarrow$	rNRPA	$1-10^{-6}$
55	pRP102	$\rightarrow$	rRP102	$1-10^{-6}$
56	pRP103	$\rightarrow$	rRP103	$1-10^{-6}$
57	pUR101	$\rightarrow$	rUR101	$1-10^{-6}$
58	pUR102	$\rightarrow$	rUR102	$1-10^{-6}$
59	pUR105	$\rightarrow$	rUR105	$1-10^{-6}$
60	pUR106	$\rightarrow$	rUR106	$1-10^{-6}$
61	pAP101	$\rightarrow$	rAP101	$1-10^{-6}$
62	pAP102	$\rightarrow$	rAP102	$1-10^{-6}$
63	pPAN101	$\rightarrow$	rPAN101	$1-10^{-6}$
64	pPAN102	$\rightarrow$	rPAN102	$1-10^{-6}$
65	pPAN103	$\rightarrow$	rPAN103	$1-10^{-6}$
66	pNOPI	$\rightarrow$	rNOPI	$1-10^{-6}$
67	rPINA	$\rightarrow$	pPINA	$1-10^{-6}$
68	rRP101	$\rightarrow$	pRP101	$1-10^{-6}$
69	rUR104	$\rightarrow$	pUR104	$1-10^{-6}$
70	rNRPA	$\rightarrow$	pNRPA	$1-10^{-6}$
71	rRP102	$\rightarrow$	pRP102	$1-10^{-6}$
72	rRP103	$\rightarrow$	pRP103	$1-10^{-6}$
73	rUR101	$\rightarrow$	pUR101	$1-10^{-6}$
74	rUR102	$\rightarrow$	pUR102	$1-10^{-6}$
75	rUR105	$\rightarrow$	pUR105	$1-10^{-6}$
76	rUR106	$\rightarrow$	pUR106	$1-10^{-6}$
77	rAP101	$\rightarrow$	pAP101	$1-10^{-6}$
78	rAP102	$\rightarrow$	pAP102	$1-10^{-6}$
79	rPAN101	$\rightarrow$	pPAN101	$1-10^{-6}$

80	rPAN102	→	pPAN102	$1-10^{-6}$
81	rPAN103	→	pPAN103	$1-10^{-6}$
82	rNOPI	→	pNOPI	$1-10^{-6}$

Remarks: Reactions 67 – 82 describe the backward reactions considered for the sensitivity studies.

Table S4. Estimated vapor pressure of HOMs at 295 K in atm.

Substance	**SIMPOL**	**COSMO-RS***	**EVAPORATION**
HO-$C_{10}H_{15}(OO)(OOH)_2$	8.82E-11	9.9E-11	5.52E-13
HO-$C_{10}H_{15}(OO)(OOH)ONO_2$	1.59E-10	8.1E-10	7.00E-11
HO-$C_{10}H_{15}(OO)(OOH)OH$	1.58E-10	2.0E-10	6.23E-12

* Estimates of COSMO-RS according to Berndt et al. (2016)

2 Results

2.1 Impact of the particle phase diffusion coefficient D_b on SOA formation

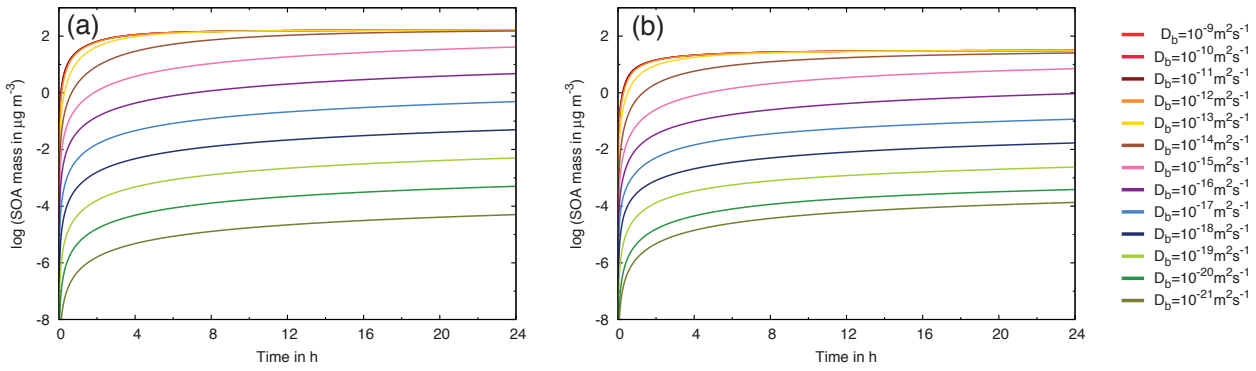

Figure S1. Simulated SOA mass for the variation of the bulk particle diffusion coefficient in the range of D_b: 10^{-9} m^2 s^{-1} – 10^{-21} m^2 s^{-1} (case 1 of Table 1) in logarithmic scale for a) $k_c = 1\,s^{-1}$ and b) $k_c = 10^{-6}\,s^{-1}$.

2.2 Impact of the mass accommodation coefficient α on SOA formation

An additional parameter influencing the SOA formation represents the mass accommodation coefficient (see Appendix A), which is defined as the probability to incorporate a molecule penetrating the particle phase boundary in the condensed phase without inducing the direct emission of a molecule of an identical type (Seinfeld and Pandis, 2006). This subsection investigates the sensitivity of SOA formation on the applied mass accommodation coefficient α. In the literature different values for the mass accommodation coefficient have been proposed for the uptake of organic compounds in organic particles/ on organic surfaces. Experimental studies show different results than model studies. Saleh et al. (2012) propose an approximate value of $\alpha = 0.4$ from evaporation studies for semi-volatile organic aerosols. In the review of Davidovits et al. (2006) concerning measured mass accommodation coefficients, the uptake values of organic species (e.g. acetic acid, α-pinene, γ-terpinene, p-cymene, and 2-methyl-2-hexanol) on 1-octanol surfaces are summarized. The mass accommodation coefficients are in the range of 0.12 and 0.4 for 265 K, whereby for α-pinene only a lower limit with $\alpha > 0.1$ is given. Moreover, Julin et al. (2014) have been combined expansion chamber measurements and molecular dynamics simulations for the determination of the mass accommodation coefficient, where bulk and surface mass accommodation coefficients have been distinguished. The probed organic substances were in liquid, semi-solid or solid phase state. Julin et al. (2014) report surface accommodation coefficients near unity ($0.96 \leq \alpha_s \leq 1$) and the bulk mass accommodation coefficients in the range of $0.14 \leq \alpha_b \leq 1$. Whereby, Julin et al. (2014) state that the conservative lower limits of the bulk mass accommodation coefficients are not very likely, due to the short simulation time scales and near unity values might be consistent with the surface mass accommodation coefficient. Additionally, the lower limit for the bulk mass accommodation coefficient assumes that adsorbed molecules will never enter

the particle bulk, and therefore, only absorbed molecules reach the particle bulk.

According to this wide spread of reported values of the mass accommodation coefficient, we varied α from 1 to 10^{-2} for all organic compounds. Further, we investigated these sensitivity studies for different bulk particle phase diffusion coefficients and pseudo-first-order rate constants of particle reactions (see model case 3a and 3b in Table 1). Fig.S2 shows the results of SOA formation for different mass accommodation coefficients and fast particle phase reactions ($k_c = 1$). The SOA mass is highest for $\alpha = 1$. For liquid aerosol particles the simulated SOA mass for $\alpha = 10^{-1}$ in fact leads to about 97 % of the formed SOA mass of the model run using $\alpha = 1$ (see Fig. S2a). For $\alpha = 10^{-2}$ the SOA mass is markedly reduced showing only about 45 % of the maximal simulated value. For nearly semi-solid aerosol particles ($D_b = 10^{-14}$ m^2 s^{-1}, see Fig. S2b) the SOA formation for $\alpha = 10^{-1}$ is reduced to 15 % of the SOA mass for the simulation with $\alpha = 1$. This demonstrates that the effect on the SOA formation is more substantial when a reduced number of molecules is transferred into the particle surface/bulk and the particle phase diffusion is slower. For semi-solid aerosols ($D_b = 10^{-18}$ m^2 s^{-1}) the simulation results are similar to those for nearly semi-solid particles with $D_b = 10^{-14}$ m^2 s^{-1} and are thus not presented. For moderate particle phase reactions the SOA formation for the reduced mass accommodation coefficients performs in the same way as for fast reactions (see Fig. S2c and S2d).

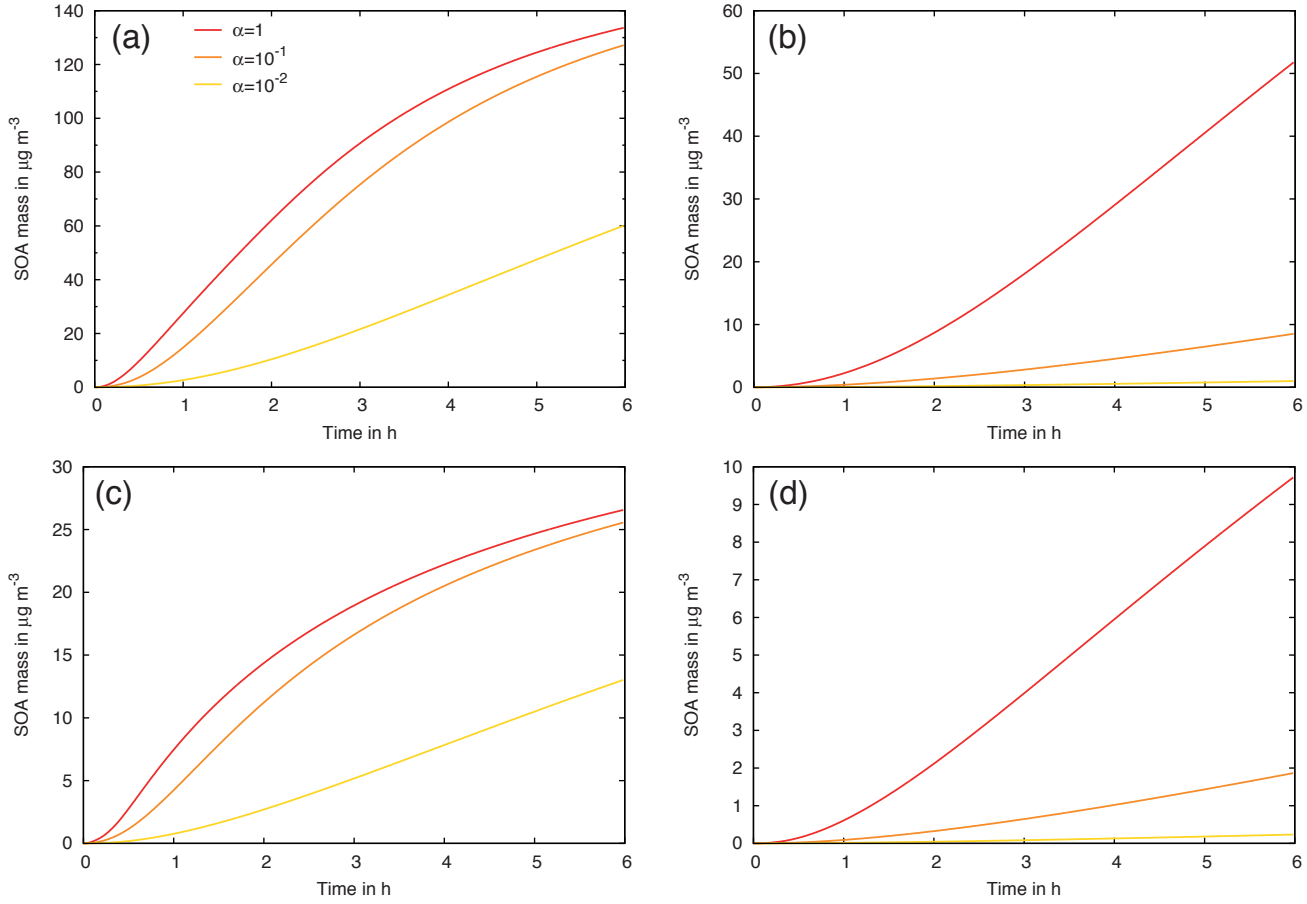

Figure S2. Simulated SOA mass for different mass accommodation coefficients for $k_c = 1\,s^{-1}$ (model case 3a of Table 1) using bulk particle diffusion coefficients for a) liquid ($D_b = 10^{-12}\,m^2\,s^{-1}$) and b) the transition between liquid and semi-solid ($D_b = 10^{-14}\,m^2\,s^{-1}$) aerosol particles and for $k_c = 10^{-4}\,s^{-1}$ (model case 3b of Table 1) using bulk particle diffusion coefficients for c) liquid ($D_b = 10^{-12}\,m^2\,s^{-1}$) and d) the transition between liquid and semi-solid ($D_b = 10^{-14}\,m^2\,s^{-1}$) aerosol particles.

2.3 Impact of the initial particle phase organic mass concentration OM_O on SOA formation

Organic material in the aerosol phase serves as an absorptive medium for organic gaseous compounds (see Eq. 4). In order to investigate the dependency of the SOA formation from the initial organic aerosol mass OM_0, the initial value has been varied from 10^{-5} to $5.8\times10^{-2}\,g\,g^{-1}$ (see Table 1, model study 5). Fig. S3 shows the results for the variation of the initial organic mass for liquid and semi-solid particles, whereby $k_c = 10^{-1}\,s^{-1}$ is held constant. For liquid particles (Fig. S3a) the initial organic mass has a marginal influence on the formed SOA mass because overall high organic mass concentrations occur for this parameter setup. For an intermediate diffusion coefficient $D_b = 10^{-14}\,m^2\,s^{-1}$ the effect of the initial organic mass is also insignificant (not shown here). For the semi-solid particles (Fig. S3b) the initial organic mass influences noticeably the formed

SOA mass. However, the total SOA mass is very low and, therefore, the relative influence of the initial organic aerosol mass is increased. The variation of the initial organic particle concentration mass has no significant influence on the formed SOA mass for aerosol particles where effective SOA formation occurs. Additionally, it is noted that a small initial organic particle mass is required for the numerical computation of the equilibrium term, otherwise the partitioning term cannot be calculated (see Eq. 4). This approach is appropriate under ambient conditions.

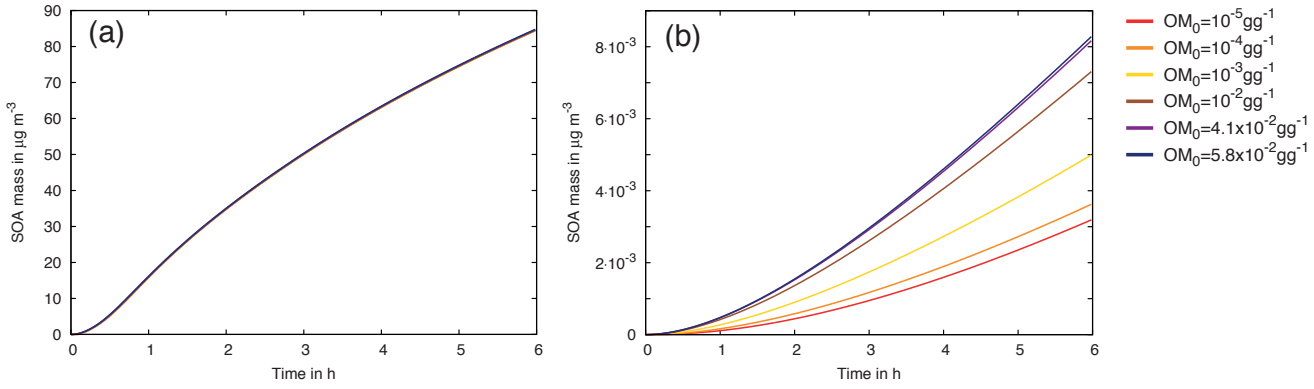

Figure S3. Simulated SOA mass formation for different initial particle phase organic mass concentrations OM_0 (model case 5 of Table 1) using diffusion coefficients of a) liquid ($D_b = 10^{-12}\,m^2\,s^{-1}$) and b) semi-solid ($D_b = 10^{-18}\,m^2\,s^{-1}$) aerosol particles.

2.4 Influence of the particle radius r_p on SOA formation

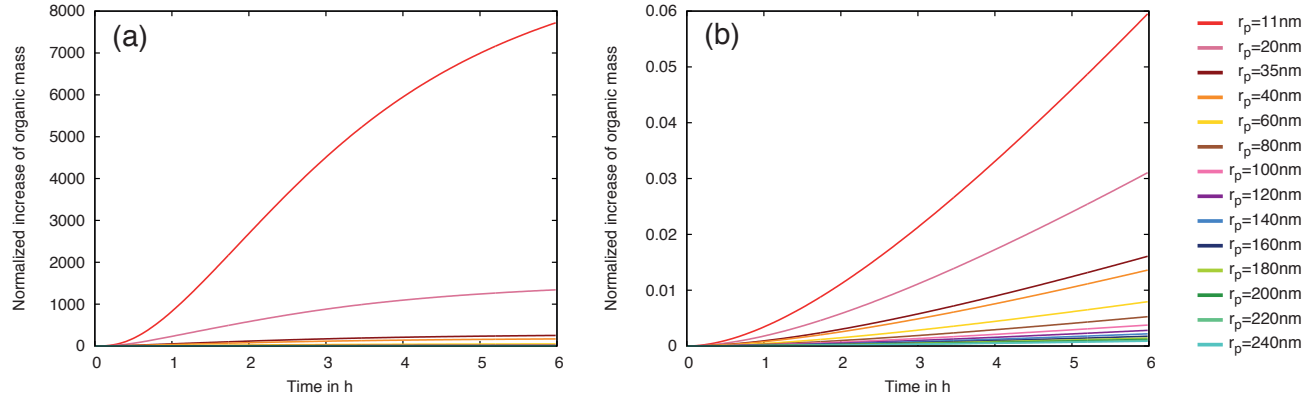

Figure S4. Normalized increase of organic mass, which describes the ratio of formed SOA and initial organic mass, for the variation of the particle radius r_p using a constant $k_c = 1\,s^{-1}$ (case 4a and 4b of Table 1); for a) liquid ($D_b = 10^{-12}\,m^2\,s^{-1}$) and b) semi-solid ($D_b = 10^{-18}\,m^2\,s^{-1}$) aerosol particles.

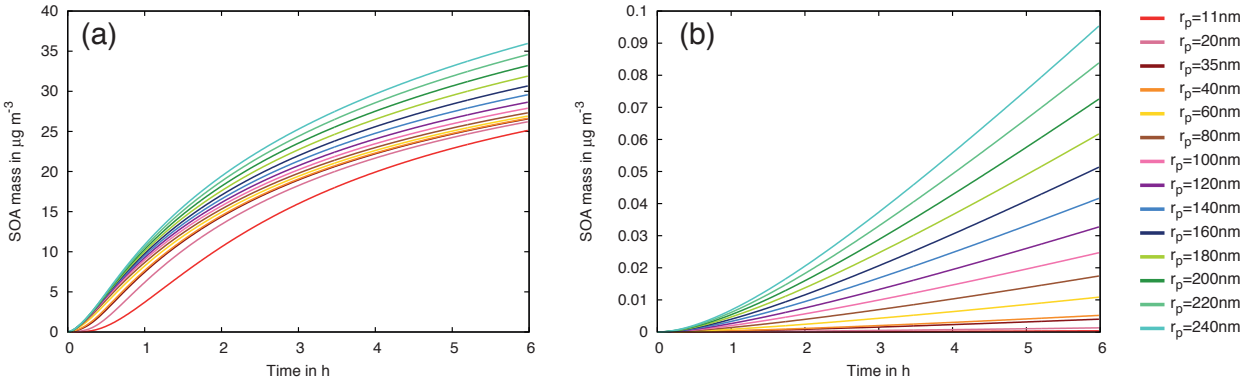

Figure S5. Results for the variation of the particle radius r_p for a constant $k_\mathrm{c} = 10^{-4}\,\mathrm{s}^{-1}$ (case 4b of Table 1) for a) liquid ($D_\mathrm{b} = 10^{-12}\,\mathrm{m}^2\,\mathrm{s}^{-1}$) and b) semi-solid ($D_\mathrm{b} = 10^{-18}\,\mathrm{m}^2\,\mathrm{s}^{-1}$) aerosol particles.

2.5 Importance of HOMs for initial SOA formation

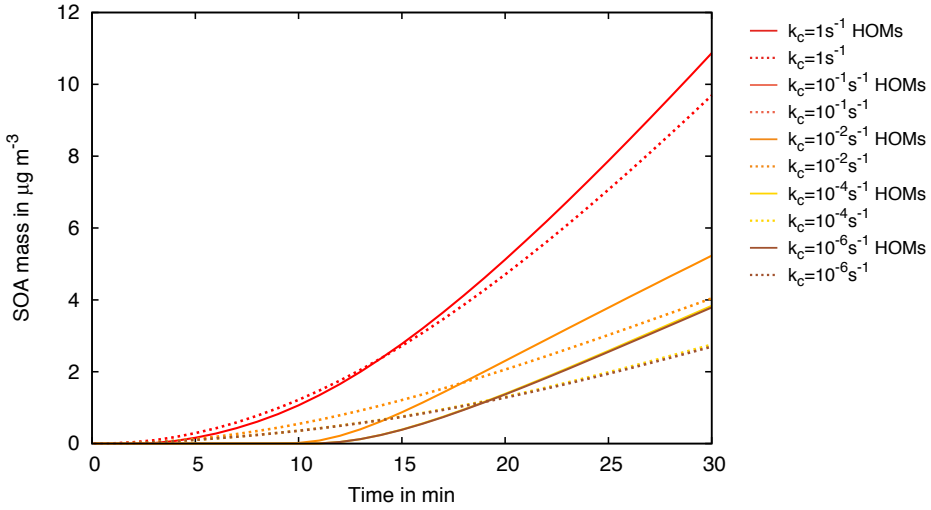

Figure S6. Simulated SOA mass including HOMs and additional variation of the pseudo-first-order rate constant of particle reactions k_c (case 6a and 6b of Table 1) for liquid ($D_\mathrm{b} = 10^{-12}\,\mathrm{m}^2\,\mathrm{s}^{-1}$) aerosol particles as shown in Fig. 4a, but only for the first half hour of the simulation time.

2.6 Implementation of a weighted particle-phase bulk diffusion coefficient

2.6.1 Calculation of the weighted particle-phase bulk diffusion coefficient

All simulations are initialized with inorganic seed particles containing water and dissolved ammonium sulfate, with a particle radius of $r_\mathrm{p} = 35\,\mathrm{nm}$. A relative humidity of 55 % leads in combination with the dissolved ammonium sulfate to the following mole fractions $x_\mathrm{inorg} = 0.43$ and $x_\mathrm{water} = 0.57$. For the self-diffusion coefficient of water, we utilize the relation proposed by Holz et al. (2000):

$$D_\mathrm{water} = D_0[(T/T_\mathrm{S}) - 1]^\gamma\,, \tag{1}$$

with:

$$D_0 = (1.635 \times 10^{-8} \pm 2.242 \times 10^{-11})\,\mathrm{m^2\,s^{-1}}\,, \tag{2}$$

$$T_\mathrm{S} = (215.05 \pm 1.20)\,\mathrm{K}\,, \tag{3}$$

$$\gamma = 2.063 \pm 0.051\,. \tag{4}$$

The self diffusion coefficients of dissolved ions are tabulated in Cussler (2009), $D_{\mathrm{NH_4^+}} = 1.96 \times 10^{-9}\,\mathrm{m^2\,s^{-1}}$ and $D_{\mathrm{SO_4^{2-}}} = 1.06 \times 10^{-9}\,\mathrm{m^2\,s^{-1}}$. For the aqueous ammonium sulfate seed particles an initial weighted particle-phase bulk diffusion coefficient of $D_\mathrm{m} = 1.78 \times 10^{-9}\,\mathrm{m^2\,s^{-1}}$ is derived. Due to the partitioning of organic compounds, the organic mole fraction x_org increases and D_org influences D_m. Since D_org is estimated to $D_\mathrm{org} = 10^{-12}\,\mathrm{m^2\,s^{-1}}$ or $D_\mathrm{org} = 10^{-14}\,\mathrm{m^2\,s^{-1}}$, the increase of the organic mole fraction causes a decrease of the weighted particle-phase bulk diffusion coefficient.

2.6.2 Evaluation of the applicability of the weighted particle-phase bulk diffusion coefficient

To evaluate the applicability of the composition dependent particle-phase bulk diffusion coefficient within the kinetic approach of Zaveri et al. (2014), comparisons of the particle-phase diffusion rate have been conducted between the semi-implicit Euler method of Zaveri et al. (2014) and the Euler forward-step method of the ETH model (Zobrist et al., 2011). For simplicity, a binary system containing water and organics is assumed. Water is treated as non-volatile (nv) and organics as semi-volatile (sv), and both are assumed to be initially completely present in the gas phase. The composition dependent particle-phase bulk diffusion coefficient is calculated with the following relation (Vignes, 1966):

$$D_\mathrm{m} = (D^0_\mathrm{sv})^{x_\mathrm{sv}} (D^0_\mathrm{nv})^{1-x_\mathrm{sv}}\,, \tag{5}$$

where, D^0_sv is the self-diffusion coefficient of the organics, D^0_nsv is the self-diffusion coefficient of water, x_sv the mole fraction of organics, and $1 - x_\mathrm{sv} = x_\mathrm{nv}$ the mole fraction of water. In the approach of Zaveri et al. (2014), the mole fraction and the diffusion coefficient are treated for the bulk, while in the approach of Zobrist et al. (2011) individual shells are considered.
For evaluation of the application of the composition dependent particle-phase bulk diffusion coefficient (Eq. 5) within the approach of Zaveri et al. (2014), the simulated particle-phase concentration of organics is compared with the results from

the ETH model. The result of the ETH model serves as standard. Fig. S7a and S7b display the model comparison for $D_{sv}^{0} = 10^{-11}\,\mathrm{m^2\,s^{-1}}$ and $D_{sv}^{0} = 10^{-13}\,\mathrm{m^2\,s^{-1}}$, respectively. The comparison indicates almost slight differences between the results of the two model approaches, whereby the bulk approach overestimates the concentration of the organics within the particle phase during the early partitioning process. The overestimation of the concentration is compensated within $1 \times 10^{-6}\,\mathrm{s^{-1}}$ and $1 \times 10^{-4}\,\mathrm{s^{-1}}$ for $D_{sv}^{0} = 10^{-11}\,\mathrm{m^2\,s^{-1}}$ and $D_{sv}^{0} = 10^{-13}\,\mathrm{m^2\,s^{-1}}$, respectively. Therefore, the application of the composition dependent particle-phase bulk diffusion coefficient following the relation of Vignes (1966) within the kinetic approach of Zaveri et al. (2014) appears as a reasonable estimate. Further, the differences for the composition dependent particle-phase diffusion coefficient are significantly smaller than for the condensation and evaporation investigations of O'Meara et al. (2017).

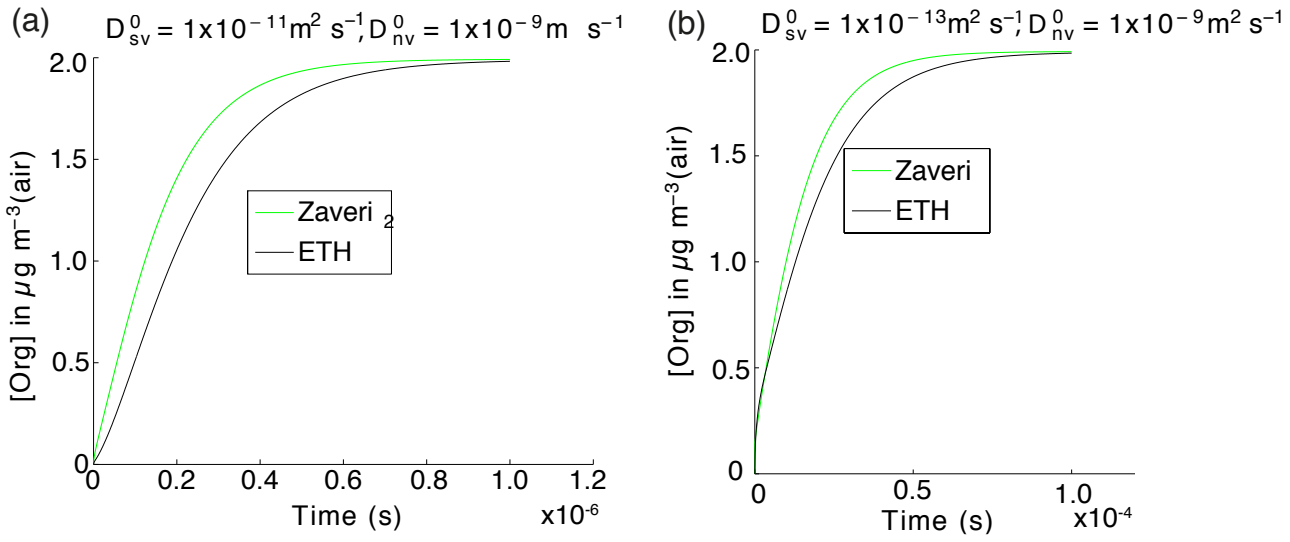

Figure S7. Model comparison of the approach from Zaveri et al. (2014) with a weighted diffusion coefficient (green line) and Zobrist et al. (2011) (gray line) for a particle phase that contains two components: water and organics with $D_{nv}^{0} = 10^{-9}\,\mathrm{m^2\,s^{-1}}$ and a) $D_{sv}^{0} = 10^{-11}\,\mathrm{m^2\,s^{-1}}$, b) $D_{sv}^{0} = 10^{-13}\,\mathrm{m^2\,s^{-1}}$, respectively. Figures courtesy of Simon O'Meara, personal communication.

2.7 Impact of different HOM vapor pressure estimates on SOA formation

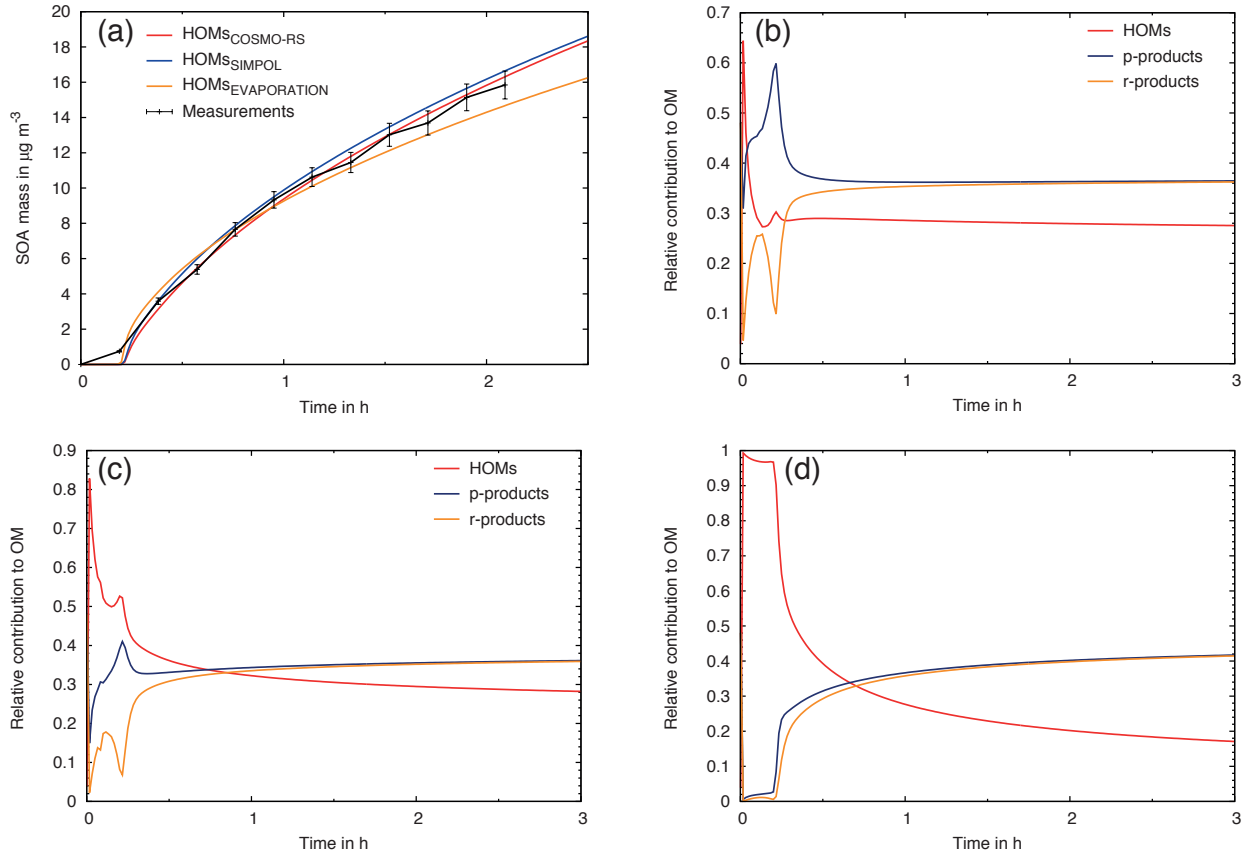

Figure S8. Results for the different vapor pressure estimates a) total SOA mass simulated with vapor pressure estimates from COSMO-RS (Eckert and Klamt, 2002), SIMPOL (Pankow and Asher, 2008) and EVAPORATION (Compernolle et al., 2011) and measured SOA mass from the experiment in LEAK. Relative contribution of the individual product classes to the total organic mass for HOM vapor pressures estimated by b) COSMO-RS c) SIMPOL d) EVAPORATION.

References

Arey, J., Aschmann, S. M., Kwok, E. S. C., , and Atkinson, R.: Alkyl Nitrate, Hydroxyalkyl Nitrate, and Hydroxycarbonyl Formation from the NO_x – Air Photooxidations of C5 – C8 n-Alkanes, The Journal of Physical Chemistry A, 105, 1020 – 1027, doi:10.1021/jp003292z, 2001.

Atkinson, R.: Gas-Phase Tropospheric Chemistry of Volatile Organic Compounds: 1. Alkanes and Alkenes, Journal of Physical and Chemical Reference Data, 26, 215 – 290, doi:10.1063/1.556012, 1997.

Berndt, T., Richters, S., Jokinen, T., Hyttinen, N., Kurtén, T., Otkjær, R. V., Kjaergaard, H. G., Stratmann, F., Herrmann, H., Sipilä, M., Kulmala, M., and Ehn, M.: Hydroxyl radical-induced formation of highly oxidized organic compounds, Nature Communications, 7, doi:10.1038/ncomms13677, 2016.

Chen, J. and Griffin, R. J.: Modeling secondary organic aerosol formation from oxidation of α-pinene, β-pinene, and d-limonene, Atmospheric Environment, 39, 7731 – 7744, doi:10.1016/j.atmosenv.2005.05.049, 2005.

Compernolle, S., Ceulemans, K., and Müller, J.-F.: EVAPORATION: a new vapour pressure estimation method for organic molecules including non-additivity and intramolecular interactions, Atmospheric Chemistry and Physics, 11, 9431 – 9450, doi:10.5194/acp-11-9431-2011, 2011.

Cussler, E. L.: Diffusion: mass transfer in fluid systems, 3rd Edition, Cambridge University Press, doi:10.1017/cbo9780511805134, 2009.

Davidovits, P., Kolb, C. E., Williams, L. R., Jayne, J. T., and Worsnop, D. R.: Mass Accommodation and Chemical Reactions at Gas-Liquid Interfaces, Chemical Reviews, 106, 1323 – 1354, doi:10.1021/cr040366k, 2006.

Eckert, F. and Klamt, A.: Fast solvent screening via quantum chemistry: COSMO-RS approach, AIChE Journal, 48, 369 – 385, doi:10.1002/aic.690480220, 2002.

Glasius, M., Calogirou, A., Jensen, N. R., Hjorth, J., and Nielsen, C. J.: Kinetic study of gas-phase reactions of pinonaldehyde and structurally related compounds, International Journal of Chemical Kinetics, 29, 527 – 533, doi:10.1002/(SICI)1097-4601(1997)29:7<527::AID-KIN7>3.0.CO;2-W, 1997.

Griffin, R. J., Dabdub, D., and Seinfeld, J. H.: Secondary organic aerosol 1. Atmospheric chemical mechanism for production of molecular constituents, Journal of Geophysical Research: Atmospheres, 107, 1 – 26, doi:10.1029/2001jd000541, 2002.

Holz, M., Heil, S. R., and Sacco, A.: Temperature-dependent self-diffusion coefficients of water and six selected molecular liquids for calibration in accurate 1H NMR PFG measurements, Physical Chemistry Chemical Physics, 2, 4740 – 4742, doi:10.1039/B005319H, 2000.

Jenkin, M. E., Saunders, S. M., and Pilling, M. J.: The tropospheric degradation of volatile organic compounds: a protocol for mechanism development, Atmospheric Environment, 31, 81 – 104, doi:10.1016/s1352-2310(96)00105-7, 1997.

Julin, J., Winkler, P. M., Donahue, N. M., Wagner, P. E., and Riipinen, I.: Near-Unity Mass Accommodation Coefficient of Organic Molecules of Varying Structure, Environmental Science & Technology, 48, 12 083 – 12 089, doi:10.1021/es501816h, 2014.

Kwok, E. S. and Atkinson, R.: Estimation of hydroxyl radical reaction rate constants for gas-phase organic compounds using a structure-reactivity relationship: An update, Atmospheric Environment, 29, 1685 – 1695, doi:10.1016/1352-2310(95)00069-B, 1995.

O'Meara, S., Topping, D. O., Zaveri, R. A., and McFiggans, G.: An efficient approach for treating composition-dependent diffusion within organic particles, Atmospheric Chemistry and Physics Discussions, 2017, 1 – 25, doi:10.5194/acp-2016-1052, 2017.

Pankow, J. F. and Asher, W. E.: SIMPOL.1: a simple group contribution method for predicting vapor pressures and enthalpies of vaporization of multifunctional organic compounds, Atmospheric Chemistry and Physics, 8, 2773 – 2796, doi:10.5194/acp-8-2773-2008, 2008.

Saleh, R., Khlystov, A., and Shihadeh, A.: Determination of Evaporation Coefficients of Ambient and Laboratory-Generated Semivolatile Organic Aerosols from Phase Equilibration Kinetics in a Thermodenuder, Aerosol Science and Technology, 46, 22 – 30, doi:10.1080/02786826.2011.602762, 2012.

Saunders, S. M., Jenkin, M. E., Derwent, R. G., and Pilling, M. J.: Protocol for the development of the Master Chemical Mechanism, MCM v3 (Part A): tropospheric degradation of non-aromatic volatile organic compounds, Atmospheric Chemistry and Physics, 3, 161 – 180, doi:10.5194/acp-3-161-2003, 2003.

Seinfeld, J. H. and Pandis, S. N.: Atmospheric Chemistry and Physics: from Air Pollution to Climate Change, 2nd Edition, John Wiley, New York, doi:10.1029/2007JD009735, 2006.

Vignes, A.: Diffusion in Binary Solutions. Variation of Diffusion Coefficient with Composition, Industrial & Engineering Chemistry Fundamentals, 5, 189 – 199, doi:10.1021/i160018a007, 1966.

Zaveri, R. A., Easter, R. C., Shilling, J. E., and Seinfeld, J. H.: Modeling kinetic partitioning of secondary organic aerosol and size distribution dynamics: representing effects of volatility, phase state, and particle-phase reaction, Atmospheric Chemistry and Physics, 14, 5153 – 5181, doi:10.5194/acp-14-5153-2014, 2014.

Zobrist, B., Soonsin, V., Luo, B. P., Krieger, U. K., Marcolli, C., Peter, T., and Koop, T.: Ultra-slow water diffusion in aqueous sucrose glasses, Phys. Chem. Chem. Phys., 13, 3514 – 3526, doi:10.1039/c0cp01273d, 2011.